JOURNAL OF SPACECRAFT AND ROCKETS
Vol. 30, No. 4, July–August 1993

Mars Environmental Survey Probe Aerobrake Preliminary Design Study

M. Tauber,* W. Henline,† and M. Chargin‡
NASA Ames Research Center, Moffett Field, California 94035
P. Papadopoulos§
Stanford University, Stanford, California 94305
Y. Chen¶
Eloret Institute, Palo Alto, California 94303
L. Yang**
Sterling Software, Palo Alto, California 94303
and
K. Hamm††
NASA Ames Research Center, Moffett Field, California 94035

The objective of this study is to design aerobrakes for the Mars Environmental Survey (MESUR) vehicles. To contain cost, existing flight-certified materials are considered for the structure and heatshield. Since the probes enter the atmosphere directly, the heatshields had to survive entry during duststorm conditions. A slightly modified Viking forebody shape, consisting of a blunted 70-deg cone, is used. An aluminum honeycomb shell is used for the structure. For the nominal 7-km/s entry, the heatshield material used on the Vikings (a silicone elastomeric charring ablator, SLA-561) was found to be lightest, yielding an aerobrake mass fraction of 13.2%. For the extreme case of entry at 9 km/s, the stagnation region heatshield consisted of the medium-density ablator AVCOAT-5026, used on the Apollo capsules, and SLA-561 was used on the conical skirt. The aerobrake mass fraction for the 9-km/s entry was 18%. The penalty resulting if a single conservatively designed aerobrake were used for both entry velocities could reach 4.8% of the entry mass at 7 km/s. Therefore, it is recommended that separate aerobrakes be designed for probes entering at 7 km/s and at 9 km/s.

Nomenclature

A	= vehicle reference area for aerodynamic coefficients, m^2
C_D	= drag coefficient
$d_{p\infty}$	= dust particle diameter at ambient conditions, μm
m	= vehicle mass at entry, kg
q	= total heat load, kJ/cm^2
p	= local surface erosion from dust particle impact
P_s	= stagnation pressure, atm
r_n	= vehicle nose radius, m
t	= time, s
V	= velocity
V_E	= entry velocity
$V_{P_{\text{imp}}}$	= velocity of impacting dust particles, m/s
γ_E	= entry flight-path angle at 125-km altitude, deg
ϵ	= emissivity of heatshield surface
ρ_t	= density of ablating heatshield material

Presented as Paper 92-2952 at the AIAA 27th Thermophysics Conference, Nashville, TN, July 6-8, 1992; received Aug. 18, 1992; revision received Oct. 30, 1992; accepted for publication Oct. 30, 1992.

*Research Scientist. Associate Fellow AIAA.
†Research Scientist. Senior Member AIAA.
‡Research Engineer. Member AIAA.
§Graduate Student, Department of Aeronautics and Astronautics. Member AIAA.
¶Research Scientist.
**Research Specialist. Member AIAA.
††Research Engineer.

Introduction

THE purpose of the Mars Environment Survey (MESUR) mission is to land a globally distributed set of 16 small, well-instrumented packages on Mars to make both short- and long-term observations of the atmosphere and the planetary surface.[1] The MESUR concept was developed at NASA Ames Research Center as a relatively low-cost, near-term approach to a Martian surface network mission that would serve both Mars science and Mission from Planet Earth objectives. MESUR is part of an evolutionary strategy for Mars exploration for two reasons: 1) in its own right, because it is accomplished over several launch opportunities and is potentially adaptive to site selection, and 2) as a precursor to a series of robotic and human missions.

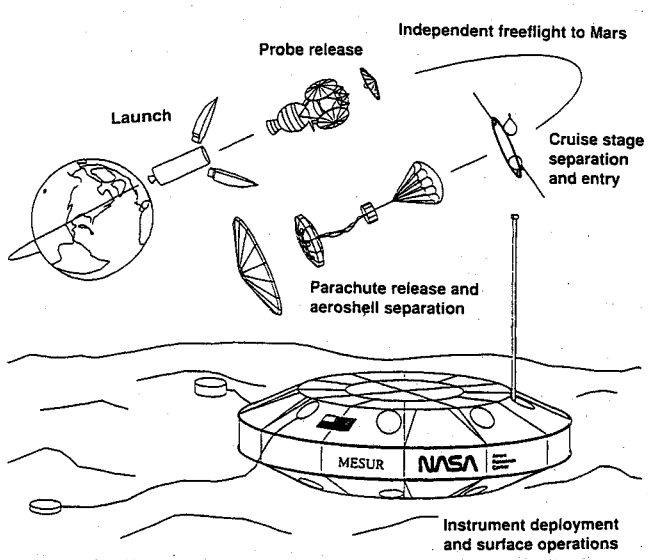

Fig. 1 MESUR mission.

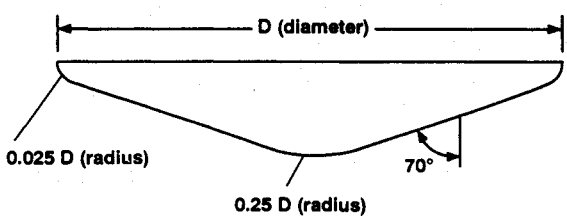

Fig. 2 Aeroshell configuration ($D = 2$ m).

The MESUR mission scenario[1] is illustrated in Fig. 1 (from Ref. 1) and assumes that each of the probes flies to Mars independently after launch. This approach (rather than using a carrier bus) has been developed to meet the targeting accuracy requirements imposed by the scientific objectives. The probes are spin stabilized, and after ground tracking, each performs course correction maneuvers on command from Earth. When the probes near Mars, they are individually tracked and further course corrections are performed to accomplish final targeting. Each probe is rotated to its entry attitude, and just before entry the cruise stage is separated. Atmospheric entry starts at an altitude of approximately 125 km. After the probe is decelerated aerodynamically to about Mach 0.8, a parachute separates the payload package from the aeroshell. The aeroshell falls to the surface, and the instrument package lands on an airbag that cushions the surface impact. After landing, the scientific instruments are deployed and start operations. The lander has the capability to communicate either directly to Earth or through a communication relay orbiter.

The design of aerobrakes for the MESUR probe is a technically challenging task. The only previous U.S. vehicles to land on Mars were the two Viking probes that entered the atmosphere from orbit at speeds of about 4.4 km/s, or roughly 60% of the mean velocity of 7 km/s for the MESUR direct entry conditions. Therefore, MESUR will experience heating rates and deceleration loads that are nearly an order of magnitude greater than those encountered by the Viking vehicles.[2]

In addition, the Viking spacecraft were propulsively decelerated into planetary orbits, and so landing times from orbit could be chosen. By contrast, MESUR's arrival window at Mars is predetermined by the launch conditions at Earth. Since the occurrence of Martian dust storms cannot be predicted, the MESUR probe's heatshield must be designed for passage through a potentially dust-laden atmosphere. Nonetheless, the Viking vehicle's forebody aerobrake shape will be used for MESUR, with minor modifications, since its high drag coefficient is aerodynamically efficient and high-speed flight data exist on the configuration.[2]

The objective of this paper is to discuss the aerobrake design process that was used for both a nominal entry velocity of 7 km/s and a high-speed case of 9 km/s. First the entry environment will be defined. Then the heating of the vehicle and the thermal protection requirements are determined for several types of heatshield materials. The structural design of the aeroshell is discussed next. Finally, the total aerobrake masses and mass fractions will be presented and discussed.

Configuration

For analysis purposes, the aerobrake's diameter was specified to be 2 m. (Viking's diameter was 3.5 m.) A 2-m diameter aeroshell is the largest body size that will permit fitting four probes into the 2.9-m diameter Delta launch vehicle shroud,[1] and it represents the "worst case" design. The forebody shape is the same as that of the Viking vehicle, with the exception of the shoulder radius that has been doubled to 5 cm to reduce the local heating rate. A sketch with relative dimensions of the MESUR forebody is shown in Fig. 2. The hypervelocity drag coefficient of this shape was calculated to be 1.7, using a Navier-Stokes code[3] with an effective specific heat ratio of 1.15.

Trajectories

The atmospheric entry trajectories were calculated assuming a spherical, nonrotating planet and the Viking atmosphere,[4,5] which has essentially the same structure as the Committee on Space Research (COSPAR) summer mean model.[5] Entry was defined (time = 0) to occur at an altitude of 125 km. Ballistic trajectories ($L/D = 0$) with an entry flight-path angle of -20 deg were used throughout. The atmospheric entry velocities ranged from 5.8 to 9 km/s. Based on an analysis of the payload and component weights, the aerobrake was sized to yield a ballistic coefficient (m/C_DA) of 30 kg/m^2. A 7-km/s entry was used as the nominal case. However, one 7- km/s entry with a ballistic coefficient of 40 kg/m^2 was also studied to determine the penalties of a potential one-third increase in vehicle mass. In addition, an entry velocity of 9 km/s, with $m/C_DA = 30$ kg/m^2, was examined. As expected, the 9-km/s entry velocity resulted in the most severe heating and pressure loads and represented a worst case design condition. The atmospheric trajectories are shown in Figs. 3 and 4. The following parameters were calculated at each point in the trajectory: 1) stagnation point convective heating for a fully catalytic, nonablating surface, 2) stagnation point equilibrium radiative heating, 3) stagnation point integrated heat loads, 4) stagnation point pressures, and 5) vehicle deceleration.

Note that the deceleration period, typically, lasted almost 40 s and the peak deceleration values occurred near an altitude of 30 km. In contrast, peak heating occurred earlier during the entry at altitudes near 40 km. The results from the trajectory calculations for the three designs that were used are listed in Table 1. (The heating calculations that were performed within the trajectory code were approximate.)

Flowfields

The flowfield about the vehicle must be known to compute the heating rates and pressure distributions, which were needed to design the heatshield and the structure. Three different numerical methods were used to solve the Navier-Stokes

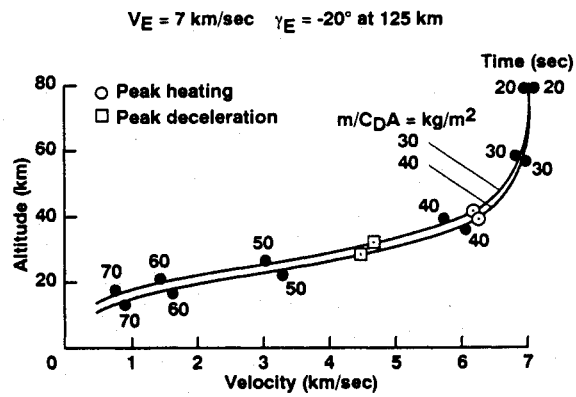

Fig. 3 MESUR entry trajectories.

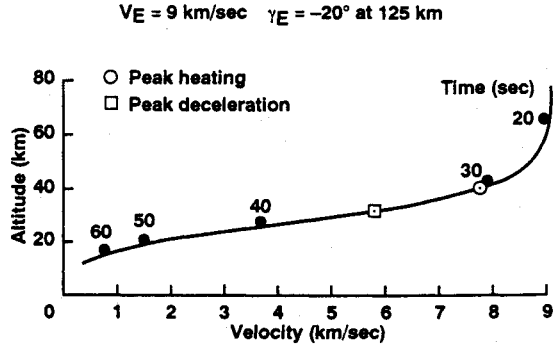

Fig. 4 MESUR entry trajectory.

Table 1 Design flight conditions

V_E km/s	m/C_DA, kg/m^2	$(dq/dt)_{max}$, W/cm^2	q, kJ/cm^2	$(dV/dt)_{max}$, m/s^2	$P_{s_{max}}$, atm
7	30	93	1.9	292	0.168
7	40	105	2.1	285	0.217
9	30	210	3.3	468	0.270

equations. In order of increasing complexity and accuracy, the methods assumed 1) an effective but constant specific heat ratio,[3] 2) the Martian atmospheric gases in thermochemical equilibrium,[6] and 3) finite chemical reaction rates and a two-temperature thermodynamic model with different translational and vibrational temperatures.[7] The three methods yielded significantly different shock-layer temperatures at high speeds. However, the pressure distributions at high speeds were nearly the same, thus facilitating the determination of structural loads. The forebody pressure distribution, computed near the peak heating point in the trajectory using method 3), is shown in Fig. 5.

Examples of the forebody shock shapes that were computed using method 2) are shown in Fig. 6 for the 7-km/s entry at two points in the trajectory. The calculations leading to the results shown in Fig. 6 also yielded shock-layer properties that were required to compute the deceleration and heating of atmospheric dust particles that impact and erode the heatshield.[6] Note the increase in the shock-layer standoff distance as the vehicle decelerated (Fig. 6). The thickening of the shock layer caused the dust particles to be decelerated more, as will be shown. Because the amount of erosion depends on the heatshield material, the erosion calculations will be included in the next section in which the vehicle's thermal protection is discussed.

Entry Thermal Protection

The MESUR probe's small size caused the primary heating mechanism to be laminar boundary-layer convection. Shock-layer radiation made only a small contribution. For example, equilibrium radiation[8] accounted for only about 1% of the stagnation point peak heating during the 7-km/s entry and less than 10% for the 9-km/s case. At locations off the stagnation point, radiation contributed even less to the heating. However, the vehicle's small size caused the boundary-layer chemistry to be "frozen," which made heatshield surface catalicity of prime importance. For example, the peak heating rates for a noncatalytic surface were only about one-half as great as those for a fully catalytic wall. Because virtually nothing is known about the actual surface catalycity of various heatshield materials in a primarily CO_2 atmosphere, by necessity the conservative fully catalytic heating rates were used in this study for design purposes. (Future intensified research in this area may provide information in time for a more detailed final design, should that be necessary.)

A reacting gas, fully viscous, shock-layer computer code developed at NASA Langley Research Center[9] was used to calculate the heating-rate distribution on the forebody. This computer program, known as viscous shock layer (VSL), provides a two-dimensional or axisymmetric simulation of the flowfield, including gas phase finite rate dissociation reactions and mass and energy diffusion under the presumption of a strong shock. A complete set of surface boundary conditions, including catalytic surface atom recombination reactions and an energy balance for a radiatively cooled wall, were imposed on the solution. (No additional boundary conditions were needed as in a boundary-layer simulation.) For the MESUR atmospheric entry, thermodynamic and transport properties for the CO_2-N_2 atmosphere were installed in the code. The knowledge of CO_2 gas phase kinetics at high temperatures is still in a preliminary state; however, the best available information was used.[10,11] An example of the heating-rate distributions is shown in Fig. 7 at the peak heating point in the 7-km/s entry trajectory. Note that the fully catalytic surface heating rates are twice as large as the noncatalytic wall rates. For the conservative design case of a fully catalytic surface, the choice of gas kinetics (values from Refs. 10 or 11) had little effect. Additional details of the flowfield and forebody heat transfer computations are given in Ref. 12.

Next, the heating-rate distributions from the VSL code were used as scaling functions in surface response and ablation calculations. Based on this information, a complete set of conduction, ablation, and thermal response computations were performed for a selected set of appropriate candidate heatshield materials.

For the two different entry velocities considered here, only the 7-km/s case offered the possibility of using a completely radiatively cooled, nonablating thermal protection system (TPS), since it was shown that the glassy surfaces of these

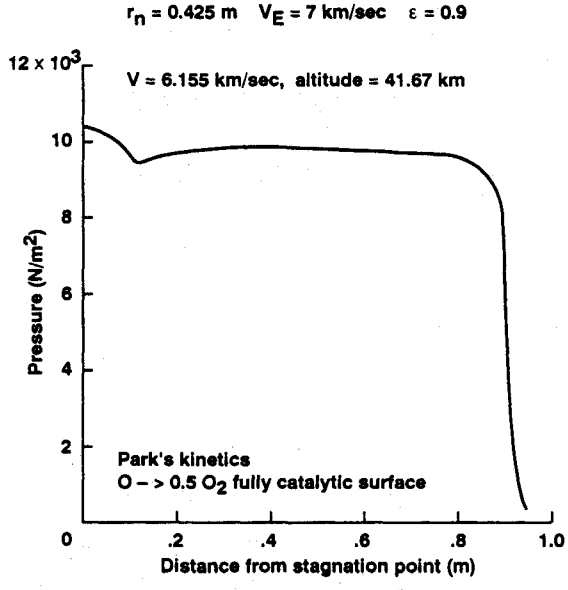

Fig. 5 Surface pressure over aeroshell.

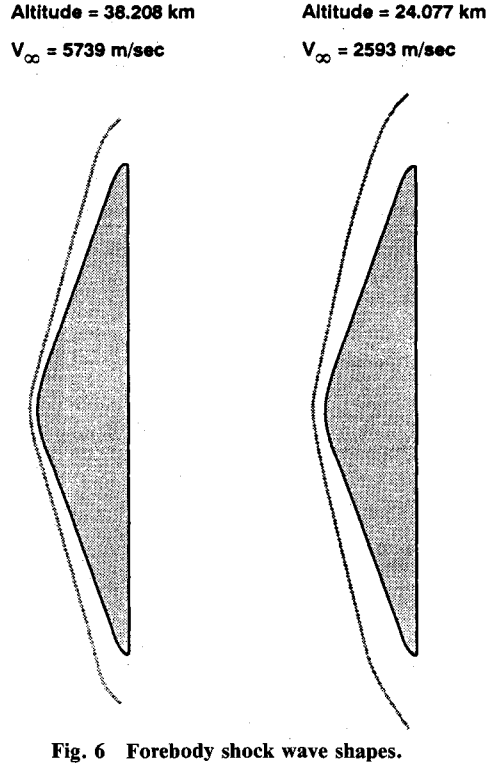

Fig. 6 Forebody shock wave shapes.

materials inhibit atom recombination; i.e., they were only partially catalytic. Because the MESUR probe must be designed (as a worst case scenario) to withstand significant surface erosion upon entry during a Martian dust storm, calculations were done here for a toughened-surface version (TUFI) of reusable surface insulation (RSI) tile known as AETB-8. This material is a matrix of silica and alumina fibers wherein the surface portion of the tile has been densified with pure silica particles. Ordinary Space Shuttle tiles are too fragile to withstand the dust particle impacts. (The atmospheric dust particle impact problem will be discussed in more detail later in this section.) In addition, the heating rates beyond the blunt nose on the conical skirt of the forebody became low enough to make AETB-8 a candidate material for the 9-km/s entry case. An in-house developed thermal conduction computer program was used to determine in-depth temperature profiles for specified TUFI tile thicknesses. It was determined that a tile layer of the minimum manufacturable thickness of 6.4 mm (0.25 in.) would give a TPS bond line temperature of less than 450 K (350°F).

In addition to RSI tile technology, an elastomeric silicone material known as SLA-561 (the heatshield material used on the Viking Mars landers built by the Martin Marietta Corp.) was considered for MESUR. The SLA-561 is a very lightweight [initial density of 232 kg/m^3 (14.5 lb/ft^3)], low-temperature, ablative material that can operate successfully to

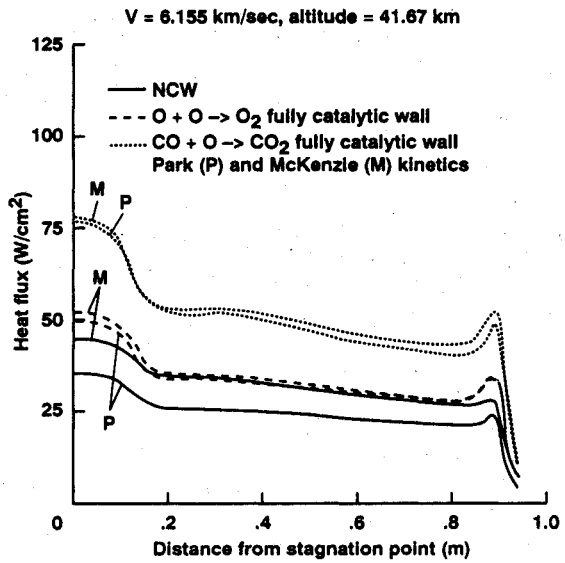

Fig. 7 Effect of surface catalysis and gas kinetics, Navier-Stokes solutions for surface heating.

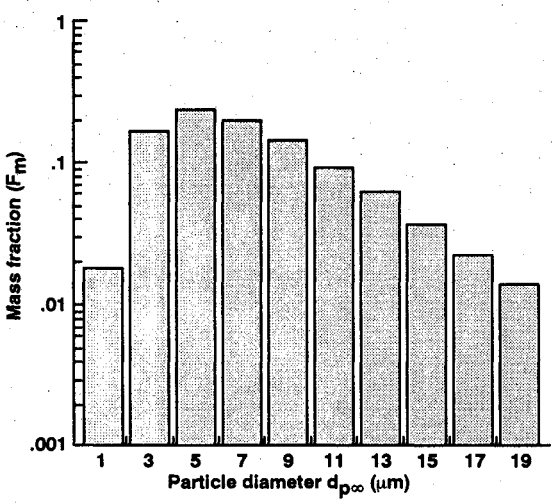

Fig. 8 Mars atmosphere dust mass fraction distribution (dust storm conditions).

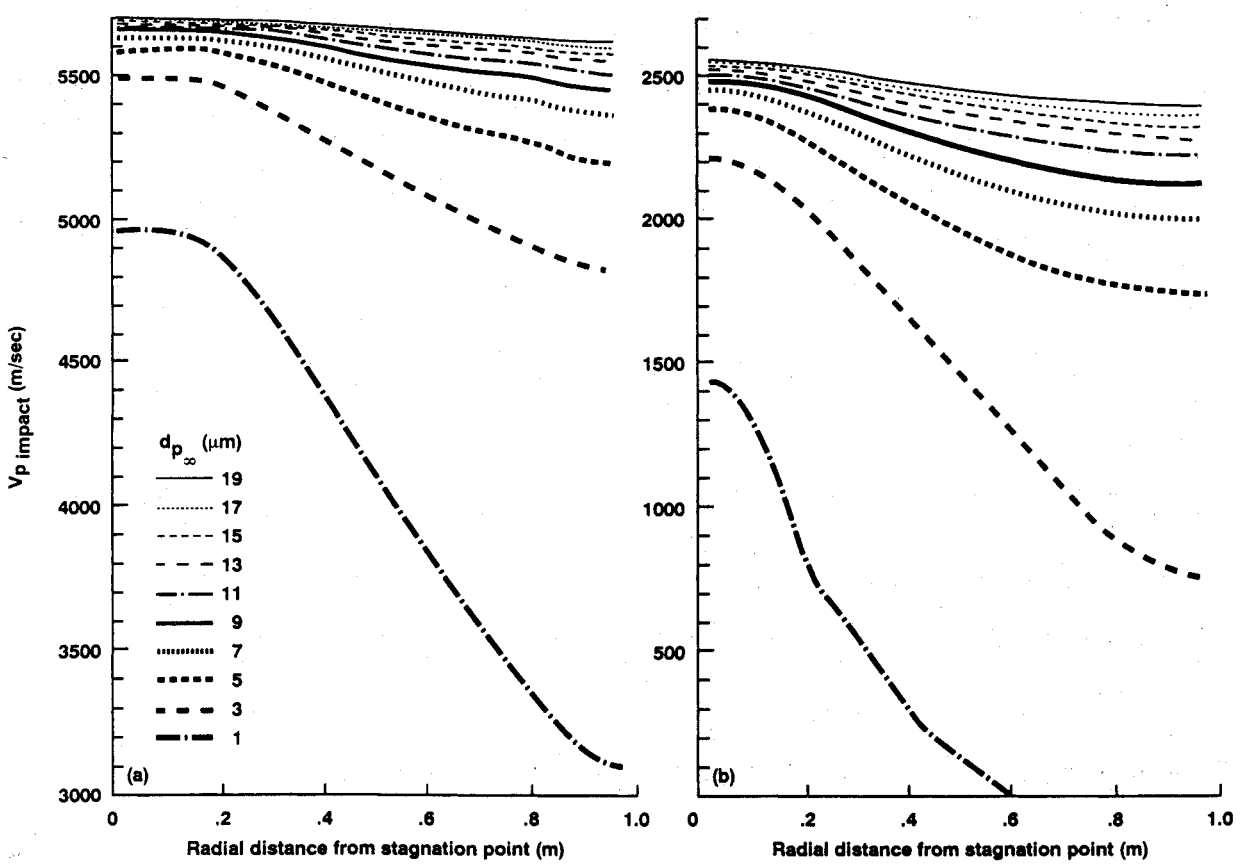

Fig. 9 Impact velocities of dust particles on heatshield: a) V_∞ = 5739 m/s, altitude = 38.3 km and b) V_∞ = 2593 m/s, altitude = 24.1 km.

heat fluxes of about 100 W/cm^2. Therefore, it was not usable in the stagnation region of the MESUR probe for the 9-km/s entry. A calculation for ablating surface recession in depth with conduction was made for the stagnation point of the MESUR probe for the 7-km/s entry using the charring material and ablation (CMA) thermal response code.[13] Results indicated that SLA-561 functioned (in this case) as a pyrolyzing (gas-producing) ablator only and experienced no surface recession from ablation. The pyrolysis gas that is produced also provides some measure of surface convective energy blockage.

In Table 1, stagnation point heat fluxes are seen to exceed 200 W/cm^2 for the 9-km/s entry. Therefore, CMA ablation thermal response calculations were also performed for a higher performance ablative TPS material known as AVCOAT-5026. This is a moderate density ablator that was used for the manned Apollo capsule heatshield material. There are many other ablation materials that could have been used here; however, almost all of those would have resulted in a significantly heavier heatshield. Thus, they were not considered further.

Mars experiences occasional global and frequent local dust storms. Following massive global storms, dust can remain in the atmosphere, to high altitudes, for weeks or months. Billions of these micron-sized particles can impact the heatshield during entry. The probability of encountering a dust-laden atmosphere at altitudes of 40 km, or even higher, was estimated[6] to be 2–4%. Therefore, it was necessary to calculate the erosion of several heatshield materials so that adequate

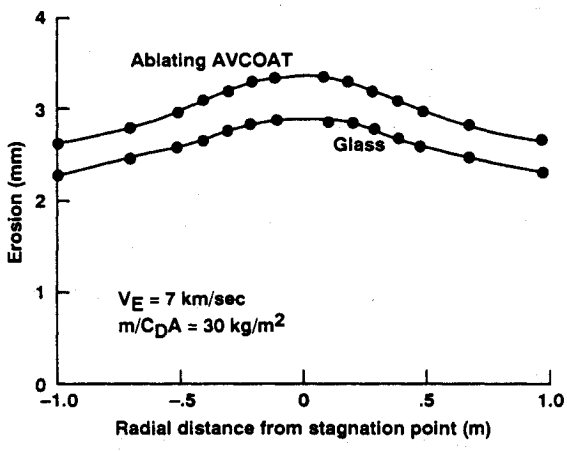

Fig. 10 Surface erosion from dust particle impacts on MESUR aeroshell.

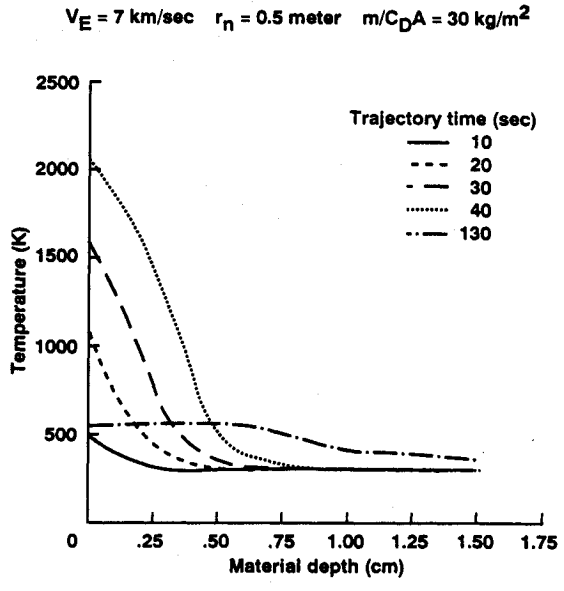

Fig. 11 MESUR probe SLA-561 thermal response.

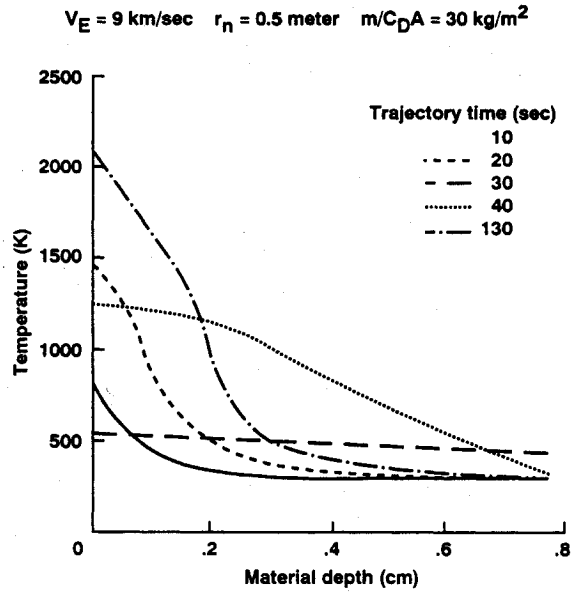

Fig. 12 MESUR probe AVCOAT thermal response.

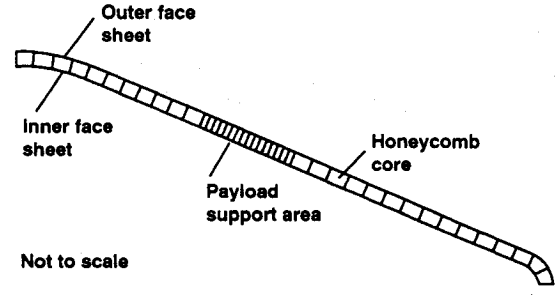

Fig. 13 Cross section of aerobrake structure.

allowances can be made in the TPS design. These calculations were very labor and computer time intensive. Therefore, heatshield erosion was computed only for glass (representative of the surface of RSI) and the ablator AVCOAT-5026 since microcratering test data were available for these two materials. The flowfield about the vehicle was calculated at nine points in the trajectory, and dust particle impact velocities and surface erosion of the heatshield were computed.[6] The atmospheric dust particle size and mass distribution[14] are illustrated in Fig. 8. The ratio of dust mass per unit volume to ambient atmospheric gas density was 10^{-4}, and this ratio was assumed to remain constant to an altitude of at least 40 km.[5]

In Fig. 9, some examples of the impact velocities of the variously sized dust particles on the heatshield are shown for the two trajectory points previously used in Fig. 6. As expected, at the lower altitude where the shock layer was thicker, the dust particles lost a larger fraction of their initial velocity. However, the shock layer was sufficiently thin so that the dust particles seldom reached their sublimation temperatures. Therefore, most of the particles had their original mass at surface impact. The dust impact velocities (Figs. 9a and 9b) were computed at the nine points in the vehicle's trajectory and were used to calculate the particles' kinetic energies, which determined the amount of heatshield erosion.

The final erosion results (Fig. 10) clearly show that RSI, which has a 0.35-mm thick glass coating, requires a toughened-surface version (TUFI). (The density of AETB-8 is substantially greater than that of RSI and offsets much of the advantage of using ceramic tiles.) For the AVCOAT ablator, the heatshield mass must be increased by about 30% to account for erosion during, or shortly after, a dust storm.

For the vehicle having a ballistic coefficient of 40 kg/m^2, the dust erosion for glass and AVCOAT was calculated using scaling laws derived previously.[6] The relation predicts that, for a body of the same size and shape making a direct atmospheric entry, the local forebody surface erosion depth from dust, Σp, will vary as

$$\Sigma p \sim (m/C_D A) V_E^2 \quad (1)$$

The dependence of erosion on the square of the entry velocity was verified when the dust impact erosion was numerically computed for the 9-km/s entry, and good agreement with Eq. (1) was found. Since microcratering data were lacking for the other heatshield materials considered here, the scaling relation[15]

$$p \sim \rho_t^{-2/3} \quad (2)$$

was used. In Eq. (2), ρ_t is the density of the charred surface heatshield material. The densities of the char layers were almost one-half those of the virgin ablators for AVCOAT-5026 and SLA-561; therefore, the erosion was increased substantially in the char layer.

The dust erosion values were added to the TPS thicknesses that were required to observe a specified bondline temperature limit. In some cases, manufacturing constraints limited the minimum TPS thickness also. Examples of temperature distributions within the heatshield are shown as a function of time from entry in Fig. 11 for the 7-km/s entry using SLA-561 for the TPS and in Fig. 12 for the 9-km/s entry vehicle with an AVCOAT heatshield. In both cases, the back surface temperatures were well below the limits for polyimide/graphite (PI/Gr) and aluminum, which are 590 K (600°F) and 505 K (450°F), respectively.

Afterbody TPS requirements were not computed, but that will be done in the future. For example, the Viking vehicles experienced afterbody heating rates that were equal to about 4% of the stagnation point values. Therefore, the peak temperatures of the surface of the payload package could reach 1000 K during the 7-km/s entry and 1200 K for the 9-km/s case. Obviously, some form of insulative TPS material will be needed to protect the payload. However, the afterbody TPS mass should be much less than that for the forebody since the heating rates are much lower and the area to be protected is far smaller.

Table 2 Result of structural optimization

Entry velocity, km/s	7.0	7.0	9.0
m/C_DA, kg/m^2	30.0	40.0	30.0
Stagnation pressure, atm	0.168	0.217	0.270
Structural mass, kg	6.22	6.76	7.80
Epoxy mass, kg	1.50	1.50	1.50
20% contingency for nonstructural components, kg	1.25	1.36	1.56
Total mass, kg	8.97	9.62	10.86
Away from support			
Outside face sheet, mm	0.254	0.254	0.254
Core thickness, mm	2.84	5.79	9.14
Inside face sheet, mm	0.254	0.254	0.279
Over the support			
Outside face sheet, mm	0.406	0.483	0.660
Core thickness, mm	2.84	5.79	9.14
Inside face sheet, mm	0.584	0.508	0.432

Structural Design

Because the structure of the aerobrake experienced primarily compression and bending, a honeycomb shell was found to be an efficient design. A PI/Gr structure was initially chosen because a bondline temperature (between the heatshield and the structure) of 590 K (600°F) could be tolerated for the brief heating period. However, in view of the scarcity of detailed information on the thermal cycle degradation and other structural properties of PI/Gr honeycomb, it was decided to also investigate, and subsequently concentrate on, the use of an all-aluminum structure. Although using AL2024 required reducing the bondline temperature limit to 505 K (450°F), the short duration of the heating pulse and the subsequent jettisoning of the aerobrake made the temperature reduction relatively unimportant. As can be seen in Figs. 11 and 12, the 505 K structural temperature limit of AL2024 was not exceeded for either the 7- or the 9-km/s entry. Although both PI/Gr and aluminum were investigated, it was decided to use AL2024 because of its well-known elevated temperature behavior, low cost, and the near-term nature of the MESUR project.

A finite element analysis was performed using the NASTRAN code.[16] The structure was divided into 69 finite elements with three variables per element consisting of the thicknesses of the inner and outer face sheets and the core of the honeycomb. To reduce the number of design variables that had to be optimized from 207 (i.e., 69 × 3) to a more tractable number, the structure was divided into two regions for analysis purposes. The first region extended from a radius of 35.23 to 52.0 cm and covered the part where the payload support ring was attached and the loads were transferred from the payload and distributed into the aeroshell. The second portion represented the remaining part of the aeroshell that was located radially inboard of 35.23 cm and outboard of 52.0 cm. This procedure resulted in reducing the variables to be optimized to five quantities. These parameters were the thicknesses of the outside and inside face sheets for each region and the core thickness (which was assumed to be the same for the entire shell but could have varying density). Two design constraints were also imposed: 1) the deflection of the structure could not exceed 6.4 mm (0.25 in.), and 2) the radii of curvature had to exceed 1.9 m.

The yield stress of AL2024-T81 is about 345 MN/m^2 (50 kpsi) when exposed to a temperature of 505 K (450°F) for one minute or so. For practical reasons, a minimum face sheet thickness of 0.25 mm (0.01 in.) was used even though the optimization calculations yielded values as low as 0.05 mm (0.002 in.) in some areas. The construction of the aeroshell was simple in theory (see Fig. 13). The face sheets were bonded to the core using polyimide epoxy. Because the loads were highest in the area where the payload support ring was attached, thicker face sheets were used to distribute the loads into the structure. It was assumed that a 0.13-mm (0.005-in.)

Table 3 Aerobrake masses and mass fractions

V_E, km/s	m/C_DA, kg/m^2	TPS type	TPS mass, kg	Structural mass, kg	Total mass, kg	% of 158-kg entry mass
7	30	AETB-8	15.6	8.97	24.57	15.55
7	30	SLA-561	11.8	8.97	20.77	13.15
7	30	SLA-561 + AETB-8	14.6	8.97	23.57	14.92
7	40	SLA-561	14.2	9.62	23.82	15.08
9	30	AVCOAT	25.4	10.86	36.26	22.95
9	30	AVCOAT + SLA-561	17.5	10.86	28.36	17.95
9	30	AVCOAT + AETB-8	21.2	10.86	32.06	20.29

thickness of epoxy on each face sheet would be sufficient. The epoxy's mass of 1.5 kg was independent of the entry velocity and the vehicle's ballistic coefficient. For example, for the nominal 7-km/s entry condition, the honeycomb core was 2.84 mm (0.112 in.) thick. The face sheet thickness was 0.254 mm (0.01 in.) except over the payload support area where the outside sheet thickness was increased to 0.406 mm (0.016 in.) and the inside sheet thickness was increased to 0.584 mm (0.023 in.) (see Table 2). Accounting for the variations of the core and face sheet thickness, adding the epoxy mass, and allowing for a 20% contingency for fasteners to attach the payload support ring and for unforeseen requirements gave the final structural masses that are listed in Table 2.

Conclusions

The total masses of the aerobrakes consisted of the sum of the TPS and the (aluminum) structural masses. Note that different combinations of TPS material were considered for each entry velocity case. The TPS mass for the vehicle having a ballistic coefficient of 40 kg/m^2 was found by scaling from the 30-kg/m^2 case. The masses that are listed in Table 3 are the final results of the current preliminary design study.

Note that the aluminum structural masses were lighter than the TPS masses for all of the cases. The lightest aerobrakes use a TPS made of SLA-561 for the 7-km/s entry and a combination of AVCOAT-5026 and SLA-561, on part of the conical skirt, for the 9-km/s entry. The difference between the masses of the lightest aerobrakes for the 7- and 9-km/s entries is about 7.6 kg. The lightest aerobrakes' mass fractions (i. e., percentage of the total vehicle's mass at entry) range from 13.15% for the nominal 7-km/s entry to 17.95% for the 9-km/s case. The penalty that would result if a single conservatively designed aerobrake were used for all MESUR probes could be as much as 4.8% of the entry mass, or nearly equivalent to the vehicle's scientific instrument payloads of 5% if the probe's 2-m diameter and ballistic coefficient of 30 kg/m^2 were held constant. Therefore, it is recommended that separate aerobrakes be designed for the probes entering at 7 and at 9 km/s.

Acknowledgments

The authors thank E. Venkatapathy and G. Candler for forebody flowfield calculations.

References

[1]Hubbard, G. S., Wercinski, P. F., Sarver, G. L., Hanel, R. P., and Ramos, R., "A Mars Environmental Survey (MESUR)—Feasibility of a Low Cost Global Approach," International Astronautical Federation, IAF Paper 91-432, Oct. 1991.

[2]Anon., "Entry Data Analysis for Viking Landers," Martin Marietta Corp., Rept. TN-3770218, Denver, CO, Nov. 1976.

[3]Venkataphathy, E., Palmer, G., and Prabhu, D. K., "AFE Base Flow Computation," AIAA Paper 91-1372, June 1991.

[4]Seiff, A., and Kirk, D. B., "Structure of the Atmosphere of Mars in Summer at Mid-Latitudes," *Journal of Geophysical Research,* Vol. 82, Sept. 1977, pp. 4364–4378.

[5]Pitts, D. E., Tillman, J. E., Johnson, N. C., Murphy, J., Pollack, J., Colburn, D. S., Haberle, R. M., Zurek, R., and Stewart, I., "The Mars Atmosphere—Observations and Model Profiles for Mars Missions," Johnson Space Center, JSC-24455, Dec. 1991.

[6]Papadopoulos, P., Tauber, M. E., and Chang, I. D., "Heat Shield Erosion in a Dusty Martian Atmosphere," AIAA Paper 92-0855, Jan. 1992.

[7]Candler, G., "Computation of Thermochemical Nonequilibrium Martian Atmospheric Entry Flows," AIAA Paper 90-1695, June 1990.

[8]Tauber, M. E., and Sutton, K., "Stagnation Point Radiative Heating Relations for Earth and Mars Entries," *Journal of Spacecraft and Rockets,* Vol. 28, No. 1, 1991, pp. 40–42.

[9]Gupta, R., and Simmonds, A., "Stagnation Flowfield Analysis for Aeroassist Flight Experiment Vehicle," AIAA Paper 88-2613, June 1988.

[10]McKenzie, R. L., "An Estimate of the Chemical Kinetics Behind Normal Shock Waves in Mixtures of Carbon Dioxide and Nitrogen for Conditions Typical of Mars Entry," NASA TN-3287, Feb. 1966.

[11]Park, C., Howe, J. T., Jaffe, R. L., and Candler, G. V., "Chemical-Kinetic Problems of Future NASA Missions," AIAA Paper 91-0464, Jan. 1991.

[12]Chen, Y. K., Henline, W. D., Stewart, D. A., and Candler, G. V., "Navier-Stokes Solutions with Surface Catalysis for Martian Atmospheric Entry," AIAA Paper 92-2946, July 1992.

[13]Kendall, R. M., Bartlett, E. P., Rindal, R. A., and Moyer, C. B., "An Analysis of the Coupled Chemically Reacting Boundary Layer and Charring Ablator (Parts I-VI)," NASA CR-1060-1065, June 1968.

[14]Toon, O.W., Pollack, J. B., and Sagan, C., "Physical Properties of the Particles Composing the Martian Dust Storm of 1971–1972," *Icarus,* Vol. 30, No. 4, 1977, pp. 663–696.

[15]Kessler, D. J., and Su, S. Y., Eds., "Hypervelocity Impact Investigations and Meteoroid Shielding Experience Related to Apollo and Skylab," *Orbital Debris,* B. G. Cour-Palais, NASA CP-2360, 1985, pp. 247–274.

[16]Anon., "MSC/NASTRAN User's Manual for Version 66," McNeil-Schwendler Corp., Los Angeles, CA, 1989.